RSC Advances

ROYAL SOCIETY OF CHEMISTRY

www.rsc.org/advances

Human Serum Albumin (HSA) Coated Liposomal Indocyanine Green for In Vivo Tumor Imaging

Siqin Chen [a], Gongjie Yu [b], Bo Zhang [b], Yinsong Wang [b], Ning Zhang [a,*], Yan Chen [b,*]

[a] Cancer Institute and Hospital, National Clinical Research Center for Cancer, Key Laboratory of Cancer Prevention and Therapy, Tianjin Medical University, Huanhuxi Road, Hexi District, 300060, People's Republic of China

[b] Research Center of Basic Medical Science & School of Pharmacy, Tianjin Key Laboratory on Technologies Enabling Development of Clinical Therapeutics and Diagnostics (Theranostics), Tianjin Medical University, No. 22 Qixiangtai Road, Heping District, Tianjin 300070, People's Republic of China

* Corresponding author:

Yan Chen

Tel.: +86-15122445834

Fax: +86-22-83336676

Email address: yxchenyan@tmu.edu.cn

Ning Zhang

Tel.: +86-13502179648

Fax: +86-22-83336676

Email address: zhangning@tijmu.edu.cn

Abstract

In this study, a near-infrared (NIR) fluorescent nanoprobe based on indocyanine green (ICG) was synthesized. In comparison with ICG solution, the resulting nanoprobe, namely HSA-Lipid-ICG NPs, exhibited remarkable improvement in stability as well as higher NIR fluorescence intensity. The in vitro experimental results demonstrated that HSA-Lipid-ICG NPs was nontoxic at physiologically relevant concentrations and could be efficiently uptaken by MCF-7 cells through endocytosis after 0.5 h incubation. The biodistribution of HSA-Lipid-ICG NPs was evaluated in mouse xenograft model. An optimized tumor contrast was observed after 8 h intravenous administration, while ICG solution had negligible effect. The tumor could be clearly detected and the signal was lasted at least up to 24 h after injection. This nanoprobe may potentially serve as an ideal contrast agent for in vivo NIR fluorescence imaging.

Introduction

Near-infrared (NIR) fluorescence imaging utilizes wavelengths in the range of 700-900 nm holds great promise as an ideal modality for cancer imaging, due to its minimal auto-fluorescence from native tissue, excellent tissue penetration ability and negligible phototoxicity[1-3]. Indocyanine green (ICG), which is the only NIR contrast agent approved for medical diagnosis by the United States Food and Drug Administration (FDA)[4], has gained much attention for applications in early detection of shallow tumors, imaging-guided tumor surgery, and tumor destruction by photothermal therapy and photodynamic therapy[4-6]. However, the use of ICG for tumor imaging applications is limited by its numerous disadvantages. In aqueous media, the amphiphilic ICG molecules suffer from aggregation induced self quenching, which leads to lower quantum yields[7]. Also, ICG is highly vulnerable to degradation when it is exposed to exterior light, oxidants and high temperatures, resulting in a loss of absorption and fluorescence[8]. Moreover, tumor localization of ICG is limited to a rather short period of time after administration due to the strong plasma protein binding of ICG and subsequent rapid clearance by the liver[8]. For the aforementioned applications, it is crucial to achieve effective ICG delivery to the tumor site and accumulation and retention of ICG in the tumor tissue. A promising approach to overcome these limitations is to encapsulate ICG within nanomaterials (*e.g.*, micelles[3], nanoparticles[9-15] and liposomes[16-18]) that provide increased stability, protection from nonspecific plasma protein binding and enhanced circulation time. Recent reports on liposomal ICG have demonstrated their potential for optical imaging of sentinel lymph nodes, vascular permeability, angiogenesis and solid tumors[16-18]. It has been found that ICG could be physically incorporated completely and stably into the lipid membrane, leading to enhanced fluorescence intensity[18].

However, the applications of conventional liposomes face challenges due to their inherent instability at the presence of serum components. Furthermore, liposomes with sub-100 nm size are prone to fuse with each other to reduce their surface tension, leading to payload loss[17,19]. To address this issue, various materials have been used to reinforce the liposome structure and provide liposomes with steric hindrance[20]. Albumin, which is the most abundant blood protein, has attracted great attention as an ideal candidate for biomedical applications due to its preferential accumulation in inflamed tissues and solid tumors, ready availability, biodegradeability, lack of inherent toxicity, immunogenicity and ability to bind to various ligands[21-22]. To the best of our knowledge, however, the use of albumin as coating material to improve the stability and biodistribution of liposomal ICG has not been reported yet.

In this work, human serum albumin (HSA) coated liposomal ICG (HSA-Lipid-ICG NPs) was synthesized and utilized for in vivo imaging of breast cancer xenograft model. The HSA shell not only can protect the liposomal ICG core from nonspecific plasma protein binding, resulted in improvement of stability of both carrier and cargo, but also can promote tumor targeting of the nanoprobe. The resulting nanoprobe was evaluated for physical and optical properties and in vitro toxicity. Finally, in vivo NIR imaging study was carried out to observe the targeting of nanoprobe to solid tumor.

Materials and methods

Materials and Regents

Cholesterol was obtained from Sigma-Aldrich Co. Ltd. (USA). Phosphatidyl ethanolamine (PE)

was obtained from Yijisy Co. Ltd. (China). Indocyanine green (ICG), 50% glutaraldehyde and absolute ethyl alcohol (EA) were obtained from J&K chemical Co. Ltd. (China). Human serum albumin (HSA) and 4% paraformaldehyde were obtained from Solarbio Co. Ltd. (USA). Penicillin-streptomycin solution (PS), 0.25% trypsin, Dulbecco minimum essential medium (DMEM) and LysoTracker Green were obtained from Life technology Co. Ltd. (USA). Fetal bovine serum (FBS) was obtained from Hyclone Co. Ltd. (USA). Cy5.5 NHS ester was obtained from GE Healthcare Co. Ltd. (USA). Hoechst 33342 was obtained from Invitrogen Co. Ltd. (USA). Cell Counting Kit-8 (CCK-8) was obtained from Dojindo laboratories (Japan).

Human breast cancer MCF-7 cell line was obtained from ATCC (USA). Cells were incubated in Dulbecco's Modified Eagle's Medium (DMEM, Life Technologies) DMEM medium containing 10% v/v fetal bovine serum (FBS) and 1% v/v penicillin/streptomycin at 37 °C with 5% CO_2. Female BALB/c nude mice with 5 weeks old were purchased from Vital River Laboratory Animal Technology Co. Ltd. (Beijing, China) and housed in a specific pathogen-reduced condition. Human breast xenograft mouse model was constructed by transplanting MCF-7 cells subcutaneously to the nude mice. All animal experiments were carried out according to the protocols approved by the Tianjin Medical University Animal Care and Use Committee.

Preparation of HSA-Lipid-ICG NPs

The liposomal ICG was firstly synthesized by the lipid film hydration and extrusion process[17]. 20 mg of PE, 1 mg of cholesterol and 0.25 mg ICG were dissolved in chloroform and mixed together. The organic solvent was evaporated under pressure using a rotary evaporator (DZF-6020, Yuhua Co. Ltd., China). The resulting thin lipid film was hydrated in ultra pure water. The obtained dispersion

was extruded through polycarbonate filters (pore size=200 nm) using a mini-extruder (Avanti Polar Lipids Co. Ltd., USA). The hydration and extrusion were performed at 60 °C, which is safely above the gel to liquid-crystalline phase transition of PE.

For HSA coating, HSA solution (pH=3.0, 2×10^{-4} mol/L) was dropwise added into aforementioned liposomal solution at a volume ratio of 1:1 and stirred for 10 minutes. HSA, coating on the liposomal surface, was then crosslinked by addition of glutaraldehyde at a final concentration of 2.5×10^{-6} mol/L for 8 h at room temperature. The resulted nanoparticle dispersion was transferred into a dialysis bag (pore size=100 kD, Solarbio Co. Ltd., USA) and purified by dialysis against PBS (pH=7.4) for 48 h.

Characterization of HSA-Lipid-ICG NPs

Size and zeta potential of nanoparticles were measured in PBS (pH=7.4) using a zetasizer system (Malvern ZS90, Malvern Co. Ltd., the United Kindom). All measurements were conducted at a backscattering angle of 173° and a temperature of 25 °C. Each measurement was repeated for three times, and the average values were taken. The morphology and structure of nanoparticles were observed by transmission electron microscope (TEM) (HT-7700, HITACHI Co. Ltd., Japan). Samples were prepared by placing a drip of latex at a concentration of 1 mg/mL onto a 400-mesh copper grid (T10023, Xinxingbairui Co. Ltd., China), followed by dropping a drip of saturated uranyl acetate for negative staining and then drying the sample at room temperature overnight.

The fluorescence measurements of ICG solution and ICG in HSA-Lipid-ICG NPs were performed on a fluorescence spectrometer (RF-5301, Shimadzu Co. Ltd., Japan) with excitation at 800 nm. Absorbance spectra of ICG solution and ICG in HSA-Lipid-ICG NPs were performed using

a UV-VIS spectrophotometer (TU-1810, Persee Co. Ltd., China). The maximum absorbance values of samples were collected to calculate UV-VIS absorbance standard curve.

The encapsulation efficiency (EE %) of ICG was calculated as follows: EE (%) = (weight of loaded ICG) / (weight of initially added ICG) ×100. The weight of loaded ICG was determined from the corresponding standard curves previously obtained by UV/VIS spectrophotometer.

In vitro drug release of HSA-Lipid-ICG NPs

To determine kinetics of ICG release from HSA-Lipid-ICG NPs and Lipid-ICG NPs, 2 ml of each sample was placed in a dialysis bag (molecular mass cut off 1000Da) and incubated in 150 ml of PBS buffer (pH=7.4) containing 10% FBS at 37 °C at the speed of 100 ± 5 rpm/min. Aliquots of incubation media were removed at each predetermined time points. The content of ICG released was determined using UV/VIS spectrophotometer. The drug release efficiency of NPs were calculated as follows: Drug release (%) = (weight of released ICG) / (weight of loaded ICG) ×100 %.

In vitro cellular uptake

For in vitro cellular uptake assay, HSA-Lipid-ICG NPs was labeled with Cy5.5-NHS ester dye at concentration of 3×10^{-5} mol/L under stirring for 24 h and then purified by dialysis against PBS (pH=7.4) for 48 h. MCF-7 cells were seeded into a 12-well chambered coverglass (NEST Co. Ltd., USA) at a density of 8000 cells per well for 12 h. The medium was replaced with serum-free DMEM with Cy5.5 labled HSA-Lipid-ICG NPs (containing 8×10^{-6} mol/L ICG). After 0 h, 0.5 h, 2 h and 6 h incubation, the cells were stained with LysoTracker Green and Hoechst 33342 for 0.5 h. The cells were then washed with PBS and fixed with 4% paraformaldehyde for 10 min. Finally, the fixed cells

were imaged by a confocal laser scanning microscope FV1000 (Olympus Co. Ltd., Japan). The fluorescence was imaged with excitation at 352 nm for hoechst 33342, at 504 nm for LysoTracker Green, and at 675 nm for Cy5.5 dye. The exposure time of different groups was fixed to obtain the change relied on time.

In vitro cytotoxicity

MCF-7 cells were seeded into 96-well plate (1×10^4 cells per well) in 200 μL of DMEM medium. Cells were incubated for 12 h to ensure the cells adhering to the bottom of plate. The media were replaced with serum-free DMEM containing either ICG solution or HSA-Lipid-ICG NPs (containing 2×10^{-7}, 1×10^{-6}, 2×10^{-6}, 1×10^{-5} and 2×10^{-5} mol/L of ICG). After 24-hour incubation, the cells were washed three times with PBS, and CCK-8 was then carried out to evaluate the cell viability. The absorbance of CCK-8 was measured at 450 nm using a microplate Bio-Rad reader (Thermo Fisher Scientific Co. Ltd., USA). The cell viability was calculated according to the following formula: cell viability (%) = $(OD_{exp}-OD_{blank}) / (OD_{control}-OD_{blank}) \times100$ %.

In vivo imaging and biodistribution studies

To construct human breast xenograft mouse model, 1×10^7 MCF-7 cells were injected to the right armpit of mice through subcutaneous injection. At two weeks after inoculation, ICG solution, Lipid-ICG NPs and HSA-Lipid-ICG NPs (0.2 mL, each containing 8×10^{-5} mol/L of ICG) were injected into MCF-7 tumor-bearing mice via tail vein. Afterwards, the biodistributions of ICG were observed at 1 h and 8 h post injections using the IVIS in vivo imaging system (PerkinElmer Co. Inc., USA). The fluorescence of ICG was collected with excitation at 745 nm and emission at 820 nm.

After 24 h post injection, the mice were sacrificed, and the major organs, including heart, liver, spleen, lung, kidneys and tumors, were collected for the further imaging.

Results and discussion

Preparation and characterization of HSA-Lipid-ICG NPs

As shown in *FIG. 1*, HSA-Lipid-ICG NPs was prepared by two steps. Lipid-ICG NPs was firstly prepared using the lipid film hydration and extrusion method. Instead of simply mixing ICG with liposome in aqueous phase, ICG and lipid were firstly mixed in an organic phase to make sure ICG was fully incorporated into the lipid membrane[18]. As shown in *FIG. 2a*, the average hydrodynamic diameter of Lipid-ICG NPs was 94.47 ± 0.13 nm and zeta potential was −43.5 ± 2.5 mV (pH=7.4). The high negative charge of Lipid-ICG NPs was believed to be contributed by ICG. The ICG encapsulation efficiency was high up to 98.2 ± 0.8 %, which was determined from the corresponding standard curves previously obtained by UV/VIS spectrometer (Supporting information, *FIG. S1*). In the second step, HSA was mixed with the Lipid-ICG NPs, and the pH value was adjusted to about 3.0, at which the HSA was positively charged due to the zwitterionic character of HSA (the isoelectric point is 5.3[23]). Thus, HSA could be easily adsorbed on the surface of Lipid-ICG NPs via electrostatic interaction. The formed HSA shell was then crosslinked by glutaraldehyde at pH 7.4. The average hydrodynamic diameter and zeta potential of resulting nanoparticles, named HSA-Lipid-ICG NPs, were 121.45 ± 0.85 nm and −32.3 ± 2.2 mV (pH=7.4), respectively. The difference in diameters between Lipid-ICG NPs and HSA-Lipid-ICG NPs demonstrated the thickness of HSA shell, which was around 30 nm.

The morphology and structure of Lipid-ICG NPs and HSA-Lipid-ICG NPs were characterized by TEM, as shown in *FIG. 2c-d*. Both Lipid-ICG NPs and HSA-Lipid-ICG NPs exhibited well-defined spherical shape and monodispersity. To verify the HSA coating, the in vitro stabilities of Lipid-ICG NPs and HSA-Lipid-ICG NPs were determined via dialysis method with 10% FBS-containing media at 37 °C, which was used to mimic the condition of blood. It is well known that serum components could disrupt liposome membranes, which would cause quick leakage of their contents[19]. Therefore, the concentration of released ICG was measured and considered as an indicator of nanoparticles degradation. As shown in *FIG. 2b*, Lipid-ICG NPs initially exhibited slow ICG release, which indicated the liposome structure remained intact. However, the stability Lipid-ICG NPs decreased after 12 h and a burst release of ICG was clearly observed. In contrast, HSA-Lipid-ICG NPs were more stable and maintained slow release of ICG for at least one week. The above results demonstrated that the HSA coating could well protect the liposomal ICG core. The long-term stability and the stable encapsulation of ICG suggested that HSA-Lipid-ICG NPs have great potential for in vivo imaging applications.

Compared with ICG solution, the HSA-Lipid-ICG NPs exhibited significant enhancement of fluorescence intensity as well as bathochromic-shift at equivalent ICG concentration (*FIG. 2e*). Similar phenomenon has been previously reported in the literature[3,24]. In the aqueous phase, the amphiphilic character of ICG leads to self-organization into aggregates caused by van der Waals forces and hydrophobic interactions[7]. Such dye-dye interactions have adverse effects on the optical properties, such as lower quantum yield due to self-quenching. The insertion of ICG within the hydrophobic domains of the lipid layer could efficiently avoid the formation of aggregates, thus

leading to a partitioning of ICG[17]. As a result, the negative effects on fluorescence properties caused by aqueous microenvironments were minimized. As shown in *FIG 2f*, after 6 days, the fluorescence intensity of ICG in HSA-Lipid-ICG NPs remained nearly 70%, while the fluorescence intensity of ICG solution decreased to almost 2%, of initially intensity. The results suggest that the fluorescence stability of ICG was significantly improved by encapsulation of HSA-Lipid-ICG NPs.

In vitro toxicity and cellular uptake

Next, the in vitro toxicity of HSA-Lipid-ICG NPs was tested in MCF-7 cells at 24 h after incubation using CCK-8 assay, and ICG solution was used as the control. As shown in *FIG. 3a*, both ICG solution and HSA-Lipid-ICG NPs exhibited no significant cytotoxicities at ICG concentrations below 8×10^{-5} mol/L, which demonstrated that the materials had good compatibility with MCF-7 cells.

The cellular uptake of HSA-Lipid-ICG NPs in MCF-7 cells was studied using confocal microscopy. In the previous investigations, both albumin nanoparticles and albumin coated nanoparticles could be uptaken by cells via endocytosis[21]. To track the HSA-Lipid-ICG NPs following their uptake, the nanoparticles were conjugated with Cy5.5 and the endo/lysosomal compartments of MCF-7 cells were stained with LysoTracker Green. As shown in *FIG. 3b*, after 0.5-hour incubation with HSA-Lipid-ICG NPs, the fluorescence of HSA-Lipid-ICG NPs (purple color) could be found and overlapped with the fluorescence of endo/lysosomes (green color), as seen by the orange areas in the merged images. It could also be found that the fluorescence intensity of nanoparticles increased with time over (*FIG. 3b*). The geometric mean fluorescence profiles of three

representative cells (pointed by arrows) were shown in *FIG. 3c*, which further illustrated that HSA-Lipid-ICG NPs could be internalized by cells as a function of time. It has been reported that the surface modification with serum albumin can accelerate the cellular uptake of nanoscale particles through clathrin-dependent endocytosis[25], which is a size-dependent process (up to 100 to 150 nm)[26]. This could be used to explain why HSA-Lipid-ICG NPs were easily internalized by tumor cells in our study. The above results indicated that HSA-Lipid-ICG NPs could be delivered into endo/lysosomes for degradation after the cellular uptake, thus provided potential in intracellular drug release.

In vivo biodistribution and tumor imaging

The feasibility of HSA-Lipid-ICG NPs for in vivo NIR fluorescence tumor imaging was then evaluated in mouse xenograft model, which was constructed by the subcutaneous injection of MCF-7 cells into the nude mice. After injection of ICG solution via tail vein, ICG was mainly distributed in the liver of MCF-7 tumor-bearing mouse after 1 h post injection and could hardly be detected after 8 h post injection (*FIG. 4a*). In plasma, ICG almost completely (98%) to serum albumin and high-density lipoproteins (HDLs)[8]. After that, ICG was excreted exclusively by liver. This behaviour causes ICG has a fast elimination from the bloodstream and a low retention rate in tumor. For Lipid-ICG NPs treated mice, the signals could be detected in major organs and tumor even after 24 h post injection which suggested that the residence time of Lipid-ICG NPs in the circulation is increased (*FIG. 4b*). However, the fluorescence intensity in tumor was too low to map the tumor. In contrast, the fluorescence signal of HSA-Lipid-ICG NPs at tumor site increased with time over, and

an optimized tumor contrast could be observed after 8 h post injection (*FIG 4c*). The ex vivo image of major organs and tumor demonstrated that HSA-Lipid-ICG NPs dramatically increased the accumulation of ICG in tumor, followed by liver (*FIG. 4c*).

We believed the enhanced and permeation effect (EPR) of solid tumors is responsible for the selective accumulation of HSA-Lipid-ICG NPs in tumor tissue. Moreover, the contribution of HSA surface coating should not be ignored. It has been reported that an albumin transport pathway mediated by gp60 located on the endothelial cell surface plays an important role for the tumor tissue distribution of albumin-bound nanoparticles. Furthermore, the SPARC (Secreted Protein, Acidic and Rich in Cysteine), a matricellular glycoprotein abundantly secreted in breast cancer, may also facilitate the transport of albumin-bound nanoparticles from extracellular matrix (ECM) to tumor cells[21].

Conclusions

In summary, we have successfully fabricated a liposomal ICG-HSA core-shell nanoprobe. Compared with ICG solution, the resulting nanoprobe exhibited remarkable enhancement in NIR fluorescence properties. The HSA shell has been proved to further improve the stability of ICG encapsulation and tumor targeting of HSA-Lipid-ICG NPs. The in vitro and in vivo experiments proved that nanoprobe was nontoxic, rapidly internalized by tumor cells and was able to image the tumor tissue. The high-performance NIR fluorescence imaging of tumor suggested the nanoprobe has great potential applications, such as intraoperative tumor visualization and early detection of tumors.

Acknowledgement

The authors thank the National High-tech R&D Program of China (863 Program 2015AA020403) and the National Natural Science Foundation of China (81472683, 81371671) for financial support.

References

1. R. Weissleder, *Nat. Biotechnol*., 2001, **19**, 316-317.
2. T. Lei, R. Manchanda, A. Fernandez-Fernandez, Y. C. Huang, D. Wright and A. J. McGoron, *RSC Adv.*, 2014, **4**, 17959-17968.
3. T. H. Kim, Y. Chen, C. W. Mount, W. R. Gombotz, X. Li and S. H. Pun, *Pharm. Res.*, 2010, **27**, 1900-1913.
4. M.L. Landsman, G. Kwant, G.A. Mook and W.G. Zijlstra, *J. Appl. Physiol.*, 1976, **40**, 575-583.
5. W. Polom, M. Markuszewski, Y.S. Rho and M. Matuszewski, *Cent. Eur. J. Urol.* 2014, **67**, 142-148.
6. D. Samorani, T. Fogacci, I. Panzini, G. Frisoni, F.G. Accardi, M. Ricci, E. Fabbri, S. Nicoletti, L. Flenghi, E. Tamburini, D. Tassinari and L. Gianni, *Eur. J. Surg. Oncol.*, 2015, **41**, 64-70.
7. R Weigand, F. Rotermund and A. Penzkofer, *Chem. Phys.*, 1997, **220**, 373-384.
8. M.A. Yaseen, J. Yu, B. Jung, M.S. Wong and B. Anvari, *Mol. Pharm.*, 2009, **6**, 1321-1332.
9. T. P. Gustafson, S. A. Dergunov, W. J. Akers, Q. Cao, S. Magalotti, S. Achilefu, E. Pinkhassik and M. Y. Berezin, *Pharm. Res.*, 2014, **3**, 5547-5555.
10. Y. Ma, S. Tong, G. Bao, C. Gao and Z. Dai, *Biomaterials*, 2013, **34**, 7706-7714.
11. M. Zheng, C. Yue, Y. Ma, P. Gong, P. Zhao, C. Zheng, Z. Sheng, P. Zhang, Z. Wang, and L. Cai, *ACS Nano*, 2013, **7**, 2056-2067.

12. P. Zhao, M. Zheng, C. Yue, Z. Luo, P. Gong, G. Gao, Z. Sheng, C. Zheng and L. Cai, *Biomaterials*, 2014, **35**, 6037-6046.

13. J. Yu, D. Javier, M. A. Yaseen, N. Nitin, R. Richards-Kortum, B. Anvari and M. S. Wong, *J. Am. Chem. Soc.*, 2010, **132**, 1929-1938.

14. B. Quan, K. Choi, Y. H. Kim, K. W. Kang and D. S. Chung, *Talanta*, 2012, **99**, 387-393.

15. V. Saxena, M. Sadoqi and J. Shao, *J. Photochem. Photobiol. B: Biol.*, 2004, **74**, 29-38.

16. S.T. Proulx, P. Luciani, S. Derzsi, M. Rinderknecht, V. Mumprecht, J.C. Leroux and M. Detmar, *Cancer Res.*, 2010, **70**, 7053-7062.

17. A. Abolfazl, R. S. Rogaie, D. Soodabeh, W. J. Sang, Z. Nosratollah, H. Younes, S. Mohammad, K. Mohammad and N. K. Kazem, *Nanoscale Res. Lett.*, 2013, **8**, 102.

18. J.C. Kraft and R.J. Ho, *Biochemistry*, 2014, **53**, 1275-1283.

19. K.I. Joo, L. Xiao, S. Liu, Y. Liu, C.L. Lee, P.S. Conti, M.K. Wong, Z. Li and P. Wang, *Biomaterials*, 2013, **34**, 3098-3109.

20. W. Gao, C. M. J. Hu, R. H. Fang and L. Zhang, *J. Mater. Chem. B*, 2013, **1**, 6569-6585.

21. B. Elsadek and F. Kratz, *J Control Release*, 2012, **157**, 4-28.

22. B. Jung and B. Anvari, *Biotechnol. Prog.*, 2012, **28**, 533-539.

23. W. Lin, A. G. A. Coombes, M. C. Davies, S. S. Davis and L. Illum, *J. Drug Target*, 1993, **1**, 237-243.

24. A.K. Kirchherr, A. Briel and K. Mader, *Mol. Pharm.*, 2009, **6**, 480-491.

25. F. Zhao, Y. Zhao, Y. Liu, Xueling Chang, C. Chen and Y. Zhao, *Small*, 2011, **7**, 1322-1337.

26. S. Zhang, J. Li, G. Lykotrafitis, G. Bao and S. Suresh, *Adv. Mater.*, 2009. **21**, 419-424.

FIG. 1. Schematic illustration of the synthesis route for HSA-coated liposomal ICG (HSA-Lipid-ICG NPs). ICG was firstly encapsulated within the liposome and HSA was then coated on the surface of the liposome.

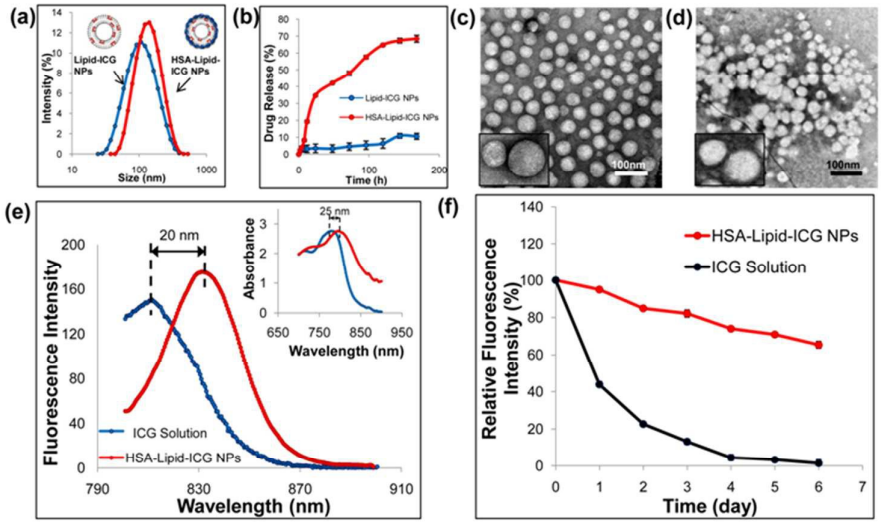

FIG. 2. Characterization of Lipid-ICG NPs and HSA-Lipid-ICG NPs. (a) Intensity size distribution of Lipid-ICG NPs and HSA-Lipid-ICG NPs measured by DLS; (b) The stability of Lipid-ICG NPs and HSA-Lipid-ICG NPs in 10% FBS solution; (c-d) TEM images of Lipid-ICG NPs and HSA-Lipid-ICG NPs (Scale bar=100 nm); (e) Fluorescence spectra with excitation at 800 nm and UV/VIS spectra of ICG solution and ICG in HSA-Lipid-ICG NPs; (f) Fluorescence stability of ICG solution and ICG in HSA-Lipid-ICG NPs.

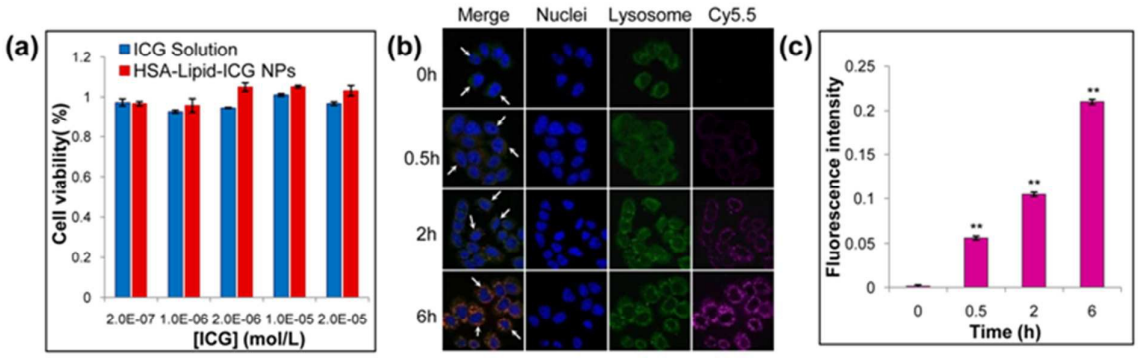

FIG. 3. *In vitro* cellular toxicity and distribution. (a) Cell survivals of MCF-7 cells after treated with different concentration of ICG solution and HSA-Lipid-ICG NPs; (b) Endocytosis of HSA-Lipid-ICG NPs. Blue represented the fluorescence of nucleus, green represented the fluorescence of lysosomes and purple reprensented the fluorescence of HSA-Lipid-ICG NPs; (c) The geometric mean fluorescence intensity of Cy5.5 stained HSA-Lipid-ICG NPs. The data were shown as mean ± SD (n=3); (**) $P < 0.01$, compared with 0-hour group.

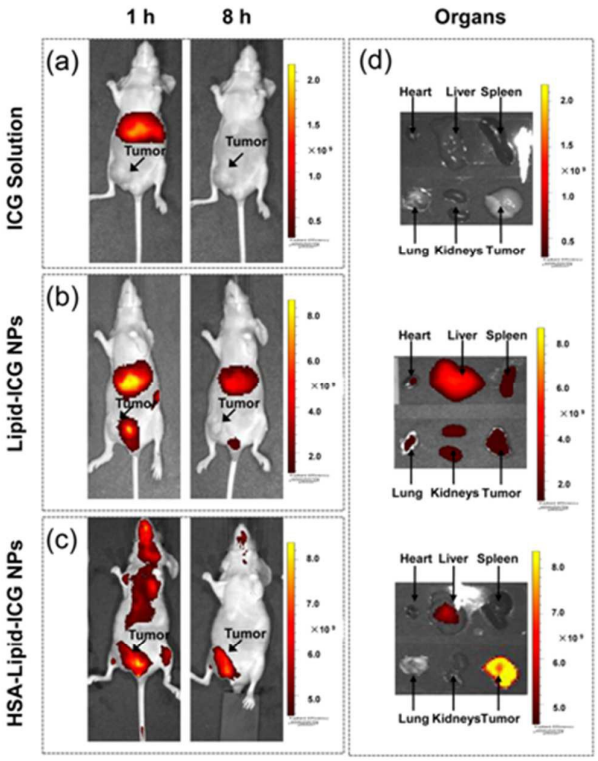

FIG. 4. In vivo fluorescence imaging and biodistribution of nude mice bearing MCF-7 tumors after intravenous injection of ICG solution, Lipid-ICG NPs and HSA-Lipid-ICG NPs. (a-c) Fluorescence images of nude mice after 1 h and 8 h post injection of ICG solution, Lipid-ICG NPs and HSA-Lipid-ICG NPs; (d) Flurorescence images of major organs and tumor tissue after injection of ICG solution, Lipid-ICG NPs and HSA-Lipid-ICG NPs at 24 h.

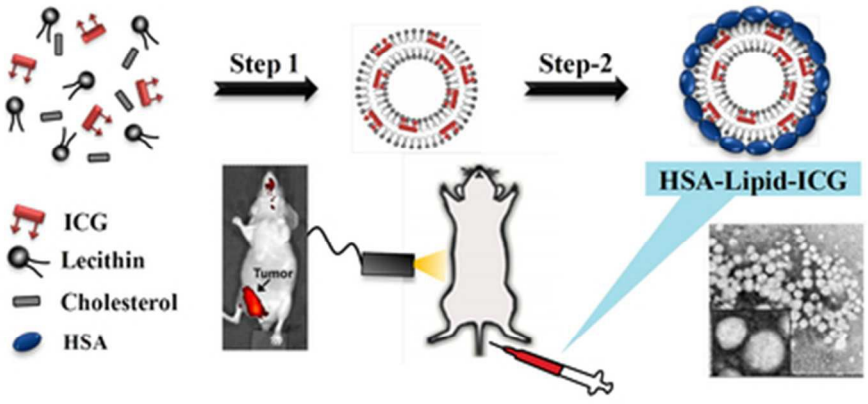

39x19mm (300 x 300 DPI)